ADVANCED MATERIALS
www.advmat.de

Joule-Heated Interfacial Catalysis for Advanced Electrified Esterification with High Conversion and Energy Efficiency

Jifang Zhang, Xinyuan Zhang, Yue Shen, Bo Fu, Yijin Wu, Jian Kang, Shan Chen, Guozhong Wang, Haimin Zhang, Huajie Yin, and Huijun Zhao**

Esterification reactions are crucial in industries such as chemicals, fragrances, and pharmaceuticals but often face limitations due to high reversibility and low reactivity, leading to restricted yields. In this work, an electrified esterification pathway utilizing a Joule-heated interfacial catalysis (JIC) system is proposed, where a hydrophilic, sulfonic acid-functionalized covalent organic framework grown on carbon felt (COF—SO_3H@CF) acts as the interfacial catalyst, and the carbon felt serves as the electric heat source. This approach achieves an acetic acid conversion of 80.5% at a heating power density of 0.49 W cm^{-3}, without additional reagents by vaporizing reaction products, surpassing the theoretical equilibrium limit of 62.5% by 1.29 times. Comprehensive analysis indicates that the intimate contact between the electric heat source and the COF—SO_3H catalyst enables efficient, localized Joule heating directly at catalytic sites, minimizing thermal losses and allowing precise control over reaction interfaces. This finding demonstrates that this JIC system not only enhances esterification efficiency but may also offer a sustainable, energy-efficient pathway for high-yield chemical processes.

1. Introduction

Conventional chemical heating relies extensively on the convection and conduction processes of heat transfer from the external devices, such as jacketed vessels or steam through a heat exchanger.[1] However, this strategy requires for a substantial temperature gradient, particularly during the bulk heating of reactants and catalyst activation, resulting in the higher construction and operational costs, as well as a larger equipment footprint.[1a,b] Electrification, including the electrochemical and electrothermal processes, is emerging as a transformative paradigm in the chemical industry, driven by the imperative to decarbonize and increase energy efficiency.[1a,b,2] Recently, the Joule heating serving as an emergency electrification thermal assist method has been proven to possess the uniform thermal field and accurate temperature control. Different with the conventional bulk heating, the Joule heating is induced by internal electric heating substrates, which could be employed to improve the electrothermal catalysis. As for the electrothermal catalysis, it could achieve the reaction interfacial heating, superior electrothermal conversion efficiency and outstanding heating rate. The localized Joule heating is only activated on the reaction interface between the catalyst and reactant, avoiding the uncontrollable limitation of thermal diffusion in bulk phase, simultaneously facilitating the reaction rate and selective catalysis. Since the excellent electrothermal conversion efficiency, the Joule-heated reaction system can be incorporated with electrically powered programmed reaction to extend the availability of renewable electricity.[1c,3] At present, this Joule heating strategy is regarded as the most promising method for electrification process, which has been successfully applied in various typical reactions, including the methane reforming/pyrolysis,[1a,c] ammonia synthesis,[1c] CO_2 reduction,[4] soot combustion,[2a] and waste plastic recycle.[5] However, the current electrothermal catalysis technology is mainly performed on the conversion of small gas molecules, while the production of fine chemicals is still limited to the traditional electrochemical and thermochemical technologies.[3a,6]

The esterification reaction between carboxylic acids and alcohols plays a pivotal role in many industries such as chemistry, fragrance, and pharmaceuticals.[7] This process is widely carried for the synthesis of chemical building blocks, biodiesel, spices, drugs, and more.[8] However, the practicality of the esterification

J. Zhang, X. Zhang, Y. Shen, Y. Wu, J. Kang, G. Wang, H. Zhang, H. Yin
Key Laboratory of Materials Physics
Centre for Environmental and Energy Nanomaterials
Anhui Key Laboratory of Nanomaterials and Nanotechnology
CAS Center for Excellence in Nanoscience
Institute of Solid State Physics
Hefei Institutes of Physical Science
Chinese Academy of Sciences
Hefei, Anhui 230031, China
E-mail: yinhj@issp.ac.cn

J. Zhang, Y. Shen, G. Wang, H. Zhang, H. Yin
University of Science and Technology of China
Hefei, Anhui 230026, China

B. Fu, J. Kang, H. Zhao
Centre for Catalysis and Clean Energy
School of Environment and Science
Griffith University Gold Coast Campus
Queensland 4222, Australia
E-mail: h.zhao@griffith.edu.au

Y. Wu
College of Chemistry and Material Science
Hengyang Normal University Hengyang
Hunan 421001, China

S. Chen
Institutes of Physical Science and Information Technology
Anhui University
Hefei, Anhui 230039, China

The ORCID identification number(s) for the author(s) of this article can be found under https://doi.org/10.1002/adma.202413949

DOI: 10.1002/adma.202413949

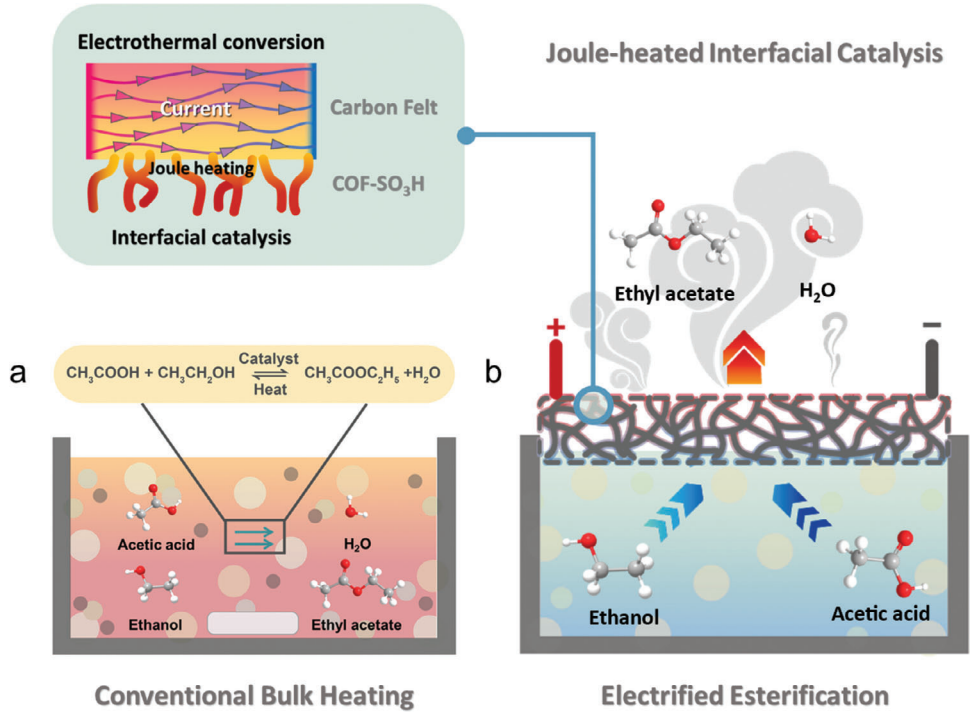

Figure 1. Schematic illustration comparing ethyl acetate preparation methods. a) Conventional Bulk Heating (CBH) method. b) Joule-heated interfacial catalysis (JIC) system for electrified esterification. Partial enlarged detail of the Joule-heated interfacial catalysis.

process faces challenges due to its inherent high reversibility and low reactivity, resulting in limited overall yields. For example, in traditional ethyl acetate (EA) production, the equilibrium conversion rate of acetic acid (AcOH) is constrained to 62.5% at a reactant molar ratio of 1:1 (EtOH:AcOH).[9] Efforts to enhance the equilibrium conversion rate generally involve the addition of excess ethanol (EtOH) and the introduction of dehydrating agents like concentrated sulfuric acid or toluene.[9,10] These supplementary reagents not only increase the reaction costs but also complicate the product separation process. Furthermore, the esterification reaction also demands elevated temperatures (60–225 °C) to expedite reaction kinetics, conventionally achieved through bulk heating methods, wherein both catalyst and reactants are heated simultaneously to the desired temperature (**Figure 1a**).[11] As esterification predominantly occurs at the catalytic sites, substantial heat is absorbed by both reactants and products in the bulk phase, resulting in large energy dissipation.[8a] Herein, we introduce an electrified esterification method that capitalizes on the novel Joule-heated interfacial catalysis (JIC) system (Figure 1b). Compared to the conventional bulk heating (CBH) system, the JIC system ingeniously combines interfacial catalysis with Joule-heated evaporation techniques to drive the esterification reaction forward efficiently. The reactants in the JIC system are pumped to the catalytic site through capillarity effect. Whereafter, the Joule heat generated by the electrothermal process acts solely on the catalytic interface, significantly avoiding the heat loss attributed to the thermal diffusion in bulk solution. Meanwhile, the products can be separated effectively to promote the esterification reaction forward, thereby breaking the theoretical equilibrium limitations of traditional esterification reactions. As illustrated in Figure 1b, the JIC system consists primarily of a porous conductive substrate and a supporting interfacial catalyst, in which the JIC system interact with the surface of the reaction liquids. As depicted in Figure 1b, reactants could swiftly diffuse along the surface of the porous conductive support, undergoing esterification at catalytic sites energized by localized Joule heating. Subsequently, products such as ester and water are detached from the catalytic interface via Joule-heated evaporation. In this case, the rapid thermal response and precise temperature control of Joule heating enable the catalytic interface to quickly reach the target reaction temperature, which maximizes heating efficiency and minimizes energy consumption. Besides, The adoption of Joule heat from the conductive substrate eliminates the need for conventional bulk heating equipment, allowing the JIC system to achieve high integration and miniaturization.

In this work, we have developed a judiciously designed JIC reactor (COF—SO_3H@CF) comprising carbon felt (CF) as a conducting support and a hydrophilic sulfonic acid-functionalized covalent organic framework (COF—SO_3H) as an interfacial catalyst for electrified esterification. By employing COF—SO_3H@CF reactor for electrified esterification of AcOH, we achieved an equilibrium conversion of 80.5%, which surpasses the theoretical equilibrium limit (62.5%) by a factor of 1.29, all without the need for additional reagents. This was accomplished at the heating power density of 0.49 W cm^{-3} and reactant molar ratio (EtOH:AcOH) of 1:1. Furthermore, the separated steam contains a high concentration of EA (88.2%), with only a small amount of EtOH (11.8%), facilitating the subsequent purification of the product. Beyond the inherent advantages of electrified esterification, our experimental and theoretical findings revealed the crucial role of hydrogen bonding interactions between the —SO_3H groups on the COF—SO_3H and the —OH groups of alcohols.

Owing to the strengthened electrostatic interaction and hydrogen bonds between the $-SO_3H$ group of COF—SO_3H and the —OH group of EtOH, the binding force between the EtOH and COF—SO_3H was stronger and made less evaporation. This approach sustains a higher concentration of reactants in proximity to the catalytic sites, while simultaneously maintaining a lower concentration of products, thus facilitating the esterification process. Additionally, we demonstrated the versatility of our JIC system (COF—SO_3H@CF) for other esterification reactions. This methodology represents a significant advancement in esterification processes, offering enhanced efficiency and precise temperature control while reducing energy consumption.

2. Results and Discussion

2.1. The Fabrication and Characterization of COF—SO_3H@CF for Electrified Esterification

In our proposed electrified esterification approach, the design of our JIC system places significant emphasis on two pivotal components: the conductive substrate and the appropriate interfacial catalyst for esterification. In terms of the conductive substrate, several key criteria must be considered: 1) high electricity-thermal conversion efficiency; 2) appropriate thermal conductivity; and 3) abundant 3D porous structure to improve the essential electric energy conversion, heat transfer, and mass transfer processes for electrified esterification. Carbon felt CF, with the suitable porous interconnected structure and electrothermal characteristics, was utilized as satisfied conductive substrate for electric Joule heating.[5,12] As depicted in Figure S1 (Supporting Information), the bare CF consists of ≈9 µm diameter carbon fibers, interlinked to form a porous 3D structure. Table S1 (Supporting Information) provides the physical characterization data, showcasing a lower volume density of CF (0.12–0.13 g cm^{-3}) compared to the conventional activated carbons (0.45–0.65 g cm^{-3}), further confirming its abundant pore structure.[13] Besides, according to the previous reports, the electrical heating technique is suited for the materials with conductivity between 0.01 and 10 S m^{-1}, while the electrical conductivity of CF is 0.2 S m^{-1}.[3b,14] As illustrated in Figure S2 (Supporting Information), CF processes the rapid thermal response upon circuit activation, reaching the desired operating temperature (≈365 K) within 38 s. This property enables precise control of localized heating conditions for interface catalysis within the JIC system.

As for the interfacial catalyst of JIC system, the sulfonic acid group-containing COF material (COF—SO_3H) was judiciously chosen as the solid acid catalyst for esterification catalysis. The chemical structure of COF—SO_3H is depicted in **Figure 2**, wherein the preserved $-SO_3H$ groups from the monomer 2,5-diaminobenzenesulfonic acid (DASA) function as the solid acid sites in COF—SO_3H, catalyzing the formation of ethyl acetate.[15] Unfortunately, COF-based solid acid catalysts have been rarely employed in conventional esterification reaction. At present, the COFs are primarily synthesized in powder form, which are hardly processable due to the insolubility and infusibility. This characteristic leads to the low utilization efficiency of active site, as well as poor electrical conductivity, thus adversely affecting the catalytic efficiency of the esterification reaction.[16] Consequently, as illustrated in Figure 2, to fabricate the COF—SO_3H@CF JIC reactor, the COF—SO_3H material was synthesized through in-situ growth on the CF substrate utilizing a hydrothermal method, which directly provides sufficient acid sites for the esterification reaction. This process involved a bulk solution containing 1,3,5-triformylphloroglucinol (Tp) and DASA as monomers, with p-toluenesulfonic acid (PTSA) serving as the catalyst. The COF—SO_3H can be formed via the Schiff-base condensation reaction between the aldehyde-group of Tp and the amine-group of DASA.[16a,17] After measurement, the loading amount of COF—SO_3H in COF—SO_3H@CF was determined as 40 mg cm^{-3}.

The morphology and nanostructure of COF—SO_3H@CF was comprehensively characterized by scanning electron microscopy (SEM). As shown in **Figure 3**a,b, the SEM images revealed that the extensive COF—SO_3H nanorods, with an average diameter of 290 nm, were uniformly distributed on the conductive CF substrate. This uniform distribution and tight contact prevent the agglomeration of COF—SO_3H, also introduce more reactive active sites, thereby promoting the catalytic ability. The corresponding cross-sectional SEM image exhibited the COF—SO_3H layer, ≈900 nm thick on the surface of CF, which could facilitate the heat transfer between the catalyst and conductive substrate. Additionally, the energy-dispersive X-ray spectroscopy (EDX) elemental mapping demonstrated the homogenous distribution of C, N, O, and S elements in COF—SO_3H@CF, indicating a comprehensive coverage of COF framework with $-SO_3H$ groups (Figure 3d). The X-ray diffraction (XRD) pattern, as depicted in Figure S3 (Supporting Information), showcases two distinct diffraction peaks at 2θ = 4.6° and 26.7°, corresponding to the (100) and (001) crystal planes of COF—SO_3H, respectively.[17,18]

The chemical structure of COF—SO_3H was measured by Fourier transform infrared spectra (FTIR), X-ray photoelectron spectroscopy (XPS) and Solid-state nuclear magnetic resonance (ssNMR). The FT-IR spectra showed the characteristic peaks at 1563 cm^{-1} (C═C) and 1194 cm^{-1} (C—N), indicating a formation of β-ketoamine linked framework structure (Figure 3e).[17] Peaks at 1431, 1079, and 1024 cm^{-1} confirmed the presence of $-SO_3H$ group.[19] The full-range XPS spectra of COF—SO_3H revealed the presence of C, N, O, and S elements (Figure 3f). High-resolution C1s and N1s XPS spectra showed the peaks of C═C—N and C—N covalent bonds, indicating condensation reactions between —CHO (Tp) and $-NH_2$ (DASA) groups (Figure S4a,b, Supporting Information).[15c,19] Similarly, high-resolution O1s and S2p XPS spectra further confirmed the presence of $-SO_3H$ groups, substantiating the successful preparation of COF—SO_3H catalyst on the CF surface (Figure S4c,d, Supporting Information).[9,17] The chemical shift of keto-form carbonyl carbon at 182.8 ppm observed in ^{13}C ssNMR spectrum verified the successful synthesis of COF—SO_3H on CF (Figure 3g).[15c] The acid density of COF—SO_3H@CF was measured at ≈0.19 mmol cm^{-3} using the NaOH titration method, demonstrating the availability of acidic sites for catalyzing esterification reactions. The loading amount of COF—SO_3H on the CF could be adjusted by varying the monomer concentrations of DASA and Tp. For example, the reactant concentrations were set at 0.5 times and 1.5 times that of COF—SO_3H@CF, denoted as COF—SO_3H@CF-1 and COF—SO_3H@CF-2. The loading amounts of COF—SO_3H in COF—SO_3H@CF-1 and COF—SO_3H@CF-2 were determined to be 24 and 80 mg cm^{-3}, respectively. SEM images (Figure S5,

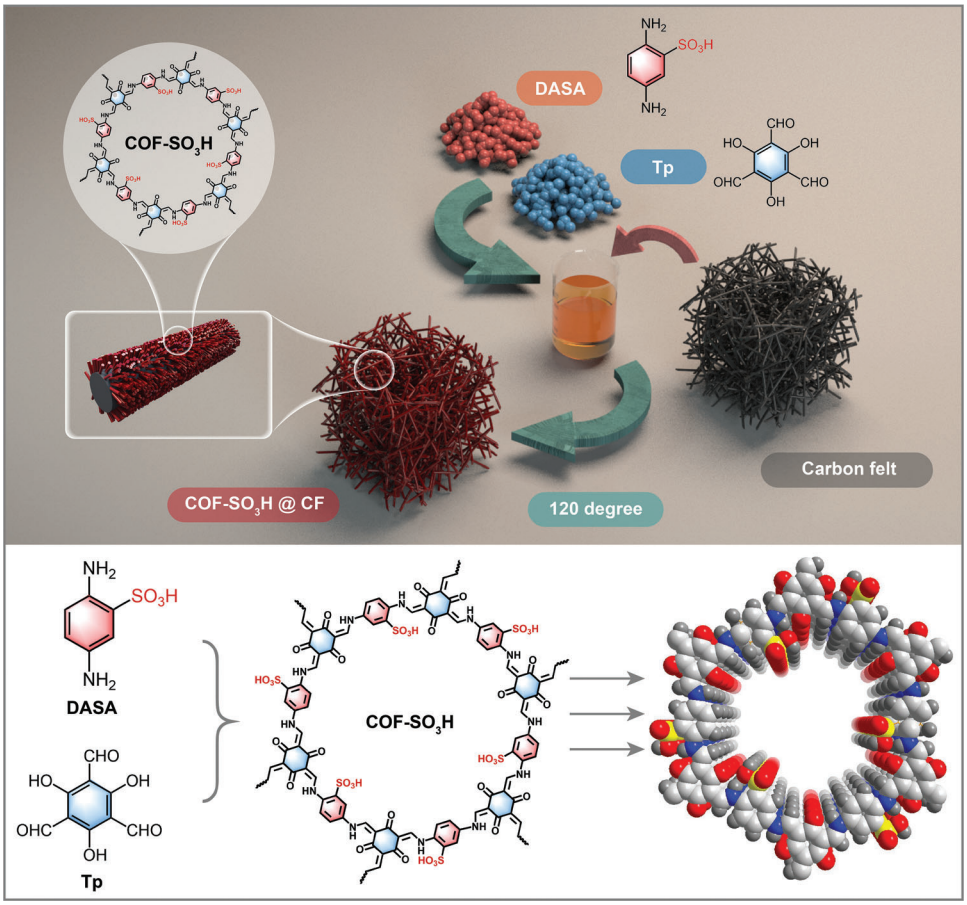

Figure 2. Schematic diagram of the preparation process for the COF—SO_3H@CF catalyst for electrified esterification. The -SO_3H groups are highlighted in red.

Supporting Information) revealed that the nanorod structures were not well-developed in either sample. The acid densities of COF—SO_3H@CF-1 and COF—SO_3H@CF-2 were 0.12 and 0.15 mmol cm^{-3} (Table S2, Supporting Information), both of which were lower than that of COF—SO_3H@CF.

In addition, the COF—SO_3H@CF exhibited a super-hydrophilic property after the growth of COFs, in contrast to the hydrophobic nature of pristine CF. As shown in Figure S6 (Supporting Information), the water contact angle of COF—SO_3H@CF approached zero, indicating that the COF—SO_3H layer significantly increased the hydrophilicity of CF substrate. The super-hydrophilic property is a crucial factor for the subsequent JIC system used in electrified esterification. During esterification, the super-hydrophilicity enhances the resultant water diffusion away from the catalytic sites of COF—SO_3H. In contrast, attributed to the inherent hydrophobicity of pristine CF, the Figure S7 (Supporting Information) exhibited numerous water beads on its surface during the esterification process. This formation of water beads on the CF surface reduces the contact area between the resultant water and CF, thereby impeding the evaporation of water species and reducing the reaction conversion rate. Overall, we successfully synthesized the COF—SO_3H catalyst with abundant acid sites and super-hydrophilic properties on CF through the hydrothermal method, which opens up the possibilities for the JIC system to achieve high equilibrium conversion rate.

2.2. The Joule-Heating Performance of COF—SO_3H@CF

The Joule-heating performance of COF—SO_3H@CF in the JIC system was first evaluated by comparing the electrothermal characteristics of CF, COF—SO_3H@CF, and COF—SO_3H@CF/Liquid (EtOH and AcOH). An optical photograph of the JIC system was shown in Figure S8 (Supporting Information), and the electric signals were recorded using a DC power supply. The surface temperature was measured with a thermal IR camera, while the internal temperature was monitored by thermocouple inserted into the CF or COF—SO_3H@CF. As displayed in Figure S9 (Supporting Information), at the same voltage, the current response of CF was higher than that of COF—SO_3H@CF. This indicates a lower ohmic resistance of CF with a dT/dq value (where q is the energy density) of 46.3 K W^{-1} cm^3 (**Figure 4a**), which generates less heat and results in worse electricity-to-thermal conversion performance. We found that the inherent ohmic resistance of COF—SO_3H@CF was increased significantly, facilitating the superior electrothermal conversion.[20] Specifically,

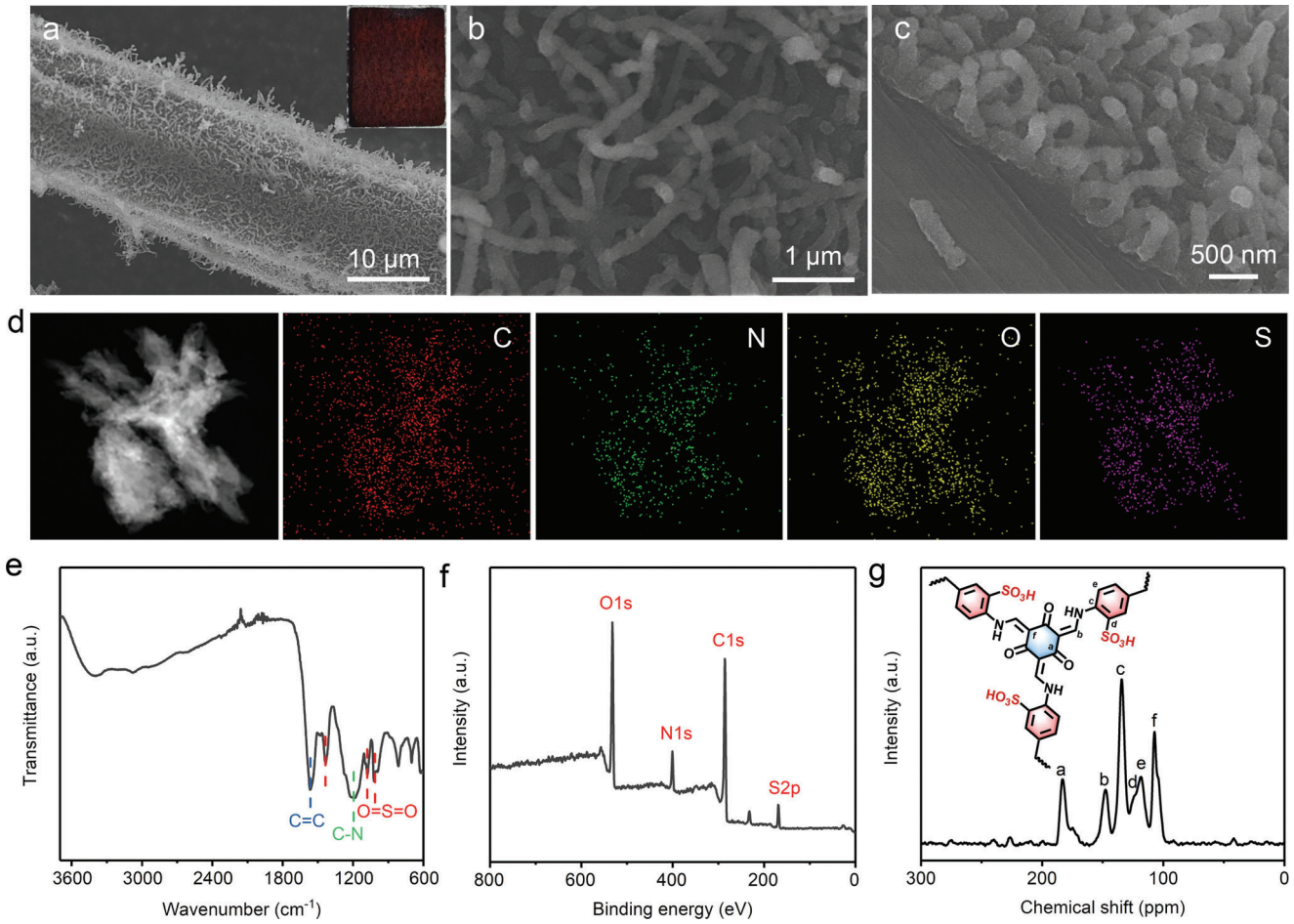

Figure 3. Characterizations of COF—SO_3H@CF catalyst. a–c) SEM images and inset photograph (inset is an optical image of COF—SO_3H@CF), d) TEM-EDS mapping, e) FT-IR spectra, f) XPS survey spectra and g) ^{13}C NMR spectra of COF—SO_3H@CF catalyst.

the value of dT/dq reached 140.5 K W^{-1} cm^3, as three times higher than that of CF (46.3 K W^{-1} cm^3, Figure 4a). When the COF—SO_3H@CF was immersed in the bulk solution (0.1 mol EtOH and 0.1 mol AcOH, ≈11.5 mL), the reactant diffused across the catalytic interface via capillary effect, subsequently occurring a heat transfer process. It is worth nothing that when the interface temperature exceeded the boiling point of 355 K for the reactant, the electrothermal conversion performance of COF—SO_3H@CF diminished, with the dT/dq value dropping to just 18.1 K W^{-1} cm^3. This is because the generated Joule heat was primarily utilized for the gasification, restricting the further increase in reaction temperature. Therefore, the JIC system can promote the esterification reactions by precisely controlling the interface temperature below 355 K, reducing heat loss due to excessively high temperatures.

To further verify the distinct electrothermal efficiency in JIC system, the Joule-heating processes were conducted in reactant solution (0.1 mol EtOH and 0.1 mol AcOH, ≈11.5 mL) with a comparison of conventional bulk heating (CBH). Notably, the temperature of COF—SO_3H@CF increased from 298 to 355 K with an input power density of 0.49 W cm^{-3} in just 29 s (Figure 4b). In contrast, the CBH system took ≈1300 s to reach the same preset temperature of 355 K with a rough input power density >10 W cm^{-3} (Figure S10, Supporting Information). The heating rate of JIC system was ≈45 times faster than that of CBH system, while requiring a lower applied energy, demonstrating a superior electrothermal conversion efficiency of COF—SO_3H@CF. The Joule heating behavior of COF—SO_3H@CF was also visualized using IR imaging (Figure 4c). It was evident that Joule heating was primarily concentrated at the catalytic interface of COF—SO_3H@CF, rather than being extensively disseminated throughout the bulk solution. The surface temperature of COF—SO_3H@CF have a swift rise from 298 to 355 K within 29 s, corroborating the temperature recorder results. Minimal changes of COF—SO_3H@CF were observed after the rapid heating process, indicating its robust thermal stability.

The current density and temperature distribution within the COF—SO_3H@CF-based JIC system were further elucidated through the finite element simulation (Figure 4d–g; Figure S11, Supporting Information). By optimizing the heating region, the effective catalyst heating area can be expanded, while simultaneously minimizing thermal energy dissipation. As illustrated in Figure 4e, the region where the graphite paper electrode contacts the COF—SO_3H@CF was defined as the heating region based on the contact height "x". Meanwhile, when

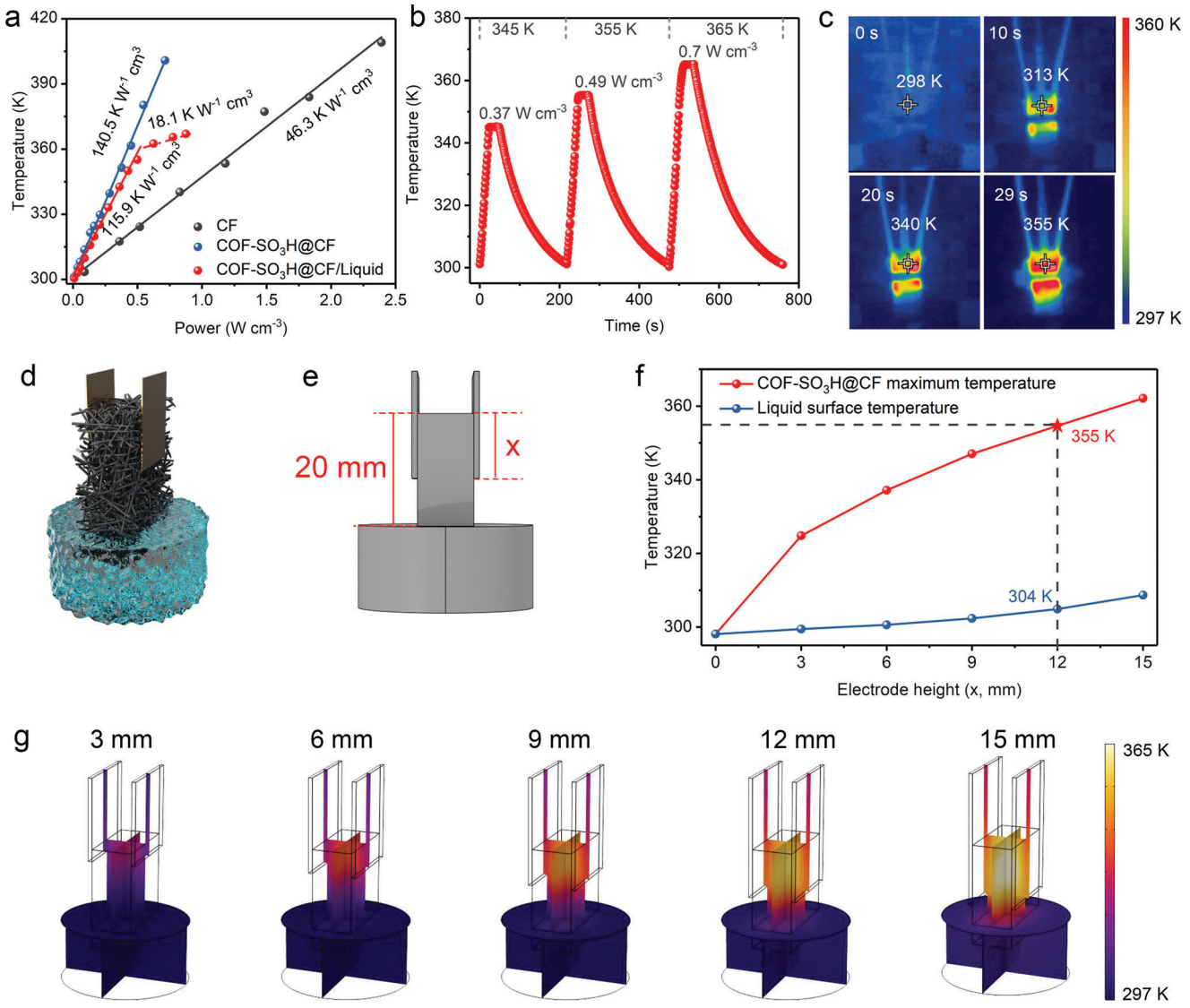

Figure 4. Electrothermal properties and simulations of the JIC system using COF—SO_3H@CF. a) The temperature-power density relationship. b) The temperature response of the JIC system with COF—SO_3H@CF. c) IR thermal images of the heating process in the JIC system with COF—SO_3H@CF. d,e) The 3D model of the JIC system with COF—SO_3H@CF. x denotes the contact height where the graphite paper electrode and the COF—SO_3H@CF. f) The maximum surface temperature of COF—SO_3H@CF and bulk solution temperature at different contact heights. g) The 3D simulation images of the temperature field in JIC system with COF—SO_3H@CF.

the graphite paper electrode was defined at contact heights of 3, 6, 9, 12, and 15 mm under the same voltage input (3.2 V), the temperature distributions of COF—SO_3H@CF were systematically investigated. The simulated results showed that the current density was predominantly distributed in the defined heating region, where generating the Joule heat flux (Figure 4g; Figure S11, Supporting Information). As the contact height increases, the COF—SO_3H@CF temperature correspondingly rises until the target reaction temperature of 355 K at a height of $x = 12$ mm (Figure 4f). Furthermore, the COF—SO_3H@CF can be heated uniformly, while the temperature fluctuation of bulk solution remains minimal and negligible. This localized heating effect, focused primarily on the catalytic interface, could significantly mitigate thermal loss and creates an energy-efficient JIC system. Thus, the JIC system using COF—SO_3H@CF provides a homogeneous thermal field and precise reaction temperature for electrified esterification processes. More importantly, it could minimize heat absorption by the bulk solution during the esterification process, thereby obviously reducing thermal energy wastage. Consequently, the selection of electrode height was set as 12 mm, for subsequent inquiry.

2.3. The Electrified Esterification Performance of COF—SO_3H@CF

The electrified esterification performances of JIC system using the COF—SO_3H@CF catalyst, as well as other comparison

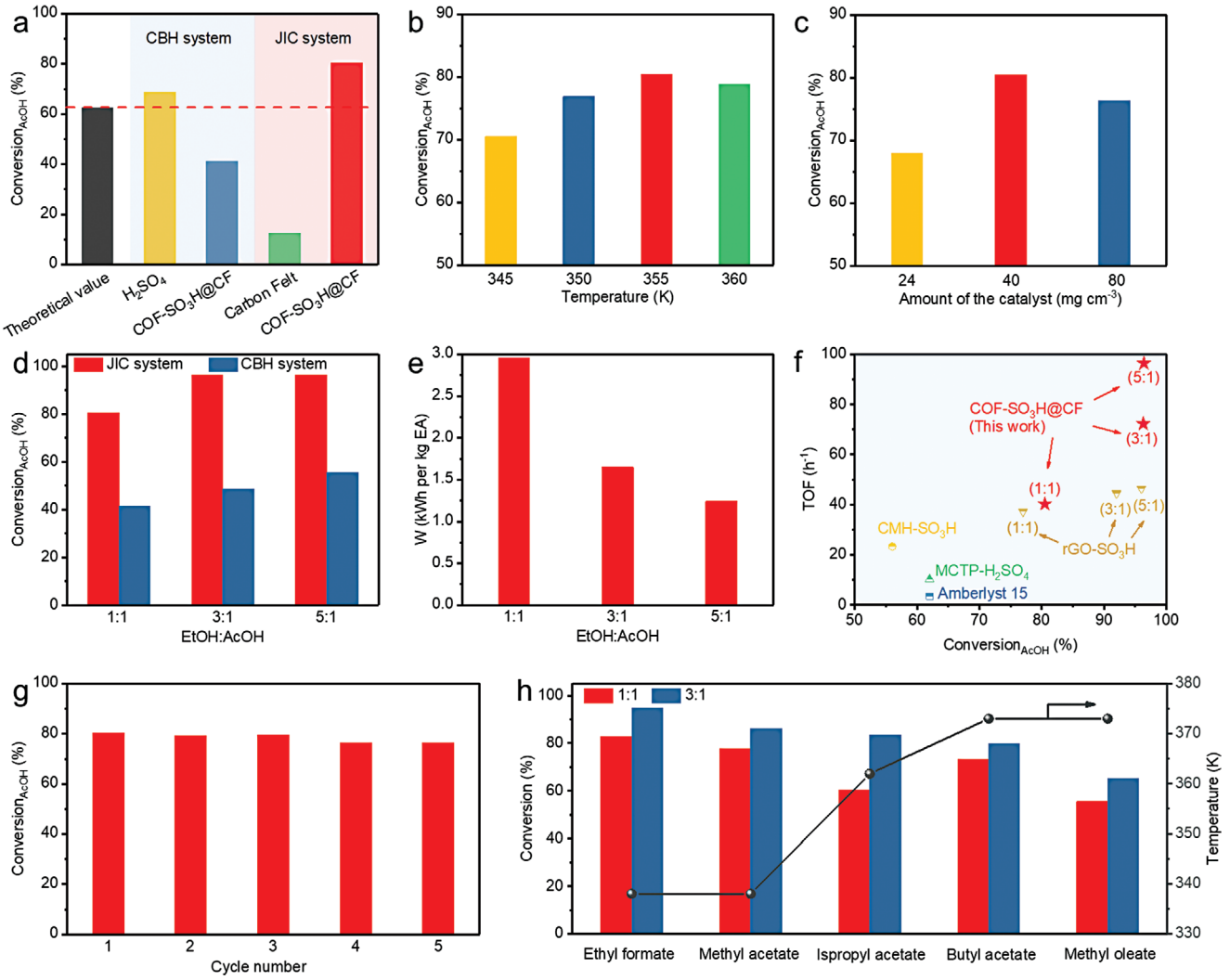

Figure 5. Evaluation of electrified esterification performance. a) Conversion rate of AcOH over different catalysts. Reaction conditions: 0.1 mol AcOH, 0.1 mol EtOH, T = 355 K, reaction time = 6 h. b–d) The conversion rate of AcOH over COF—SO_3H@CF with (b) different reaction temperature, c) catalyst loading amount and d) molar ratios of EtOH to AcOH. e) Electricity consumption per kg_{EA} in the JIC system with different molar ratios of EtOH to AcOH. f) Comparison of conversion rate for AcOH and the turnover frequency value among the catalysts reported in Table S3 (Supporting Information). g) The stability test of COF—SO_3H@CF for 5 times in the JIC system. h) Conversion rate of different substrates in the JIC system.

catalysts, were evaluated in a custom-built chemical reactor (Figure S8, Supporting Information). Initially, we focused on the model esterification reaction of EtOH and AcOH. In our JIC system, the product EA was generated in situ on the surface/acidic sites and then rapidly evaporated away from the electrothermal localized surface. As depicted in **Figure 5a**, the equilibrium conversion rate of JIC system using pristine CF was only 12.5% at a 1:1 reactant molar ratio of EtOH and AcOH. This low conversion rate was primarily attributed to absence of catalytic sites in CF, resulting in the negligible catalytic ability of bare CF and poor esterification performance. In contrast, the application of COF—SO_3H@CF catalyst resulted in a higher conversion efficiency of 80.5%, surpassing both the theoretical equilibrium conversion rate (62.5%) and that catalyzed by concentrated sulfuric acid (68.9%). This excellent conversion performance highlights the superior capability of COF—SO_3H@CF catalyst in enhancing the equilibrium conversion rate of esterification reaction. To further verify the advantages of JIC system in esterification reactions, a comparative analysis for the CBH system was conducted. In the CBH system, the equilibrium conversion rate catalyzed by COF—SO_3H@CF was restricted to 39.0%, significantly lower than the 80.5% obtained in the JIC system. This emphasized the pivotal role of the JIC system in augmenting esterification reaction performance. Temperature regulation within the JIC system also acts as a critical factor. Figure 5b illustrates the volcanic trend in AcOH equilibrium conversion rate with increased temperature in our JIC system using COF—SO_3H@CF. After 6 h of stable operation at 355 K, the conversion of AcOH was 80.5%, with a required heating power density of 0.49 W cm^{-3} (Figure S12, Supporting Information). In this case, the rate constant of the reaction is 0.051 L mol^{-1} h^{-1} (Figure S13, Supporting Information). Thus, the esterification of AcOH and EtOH can be

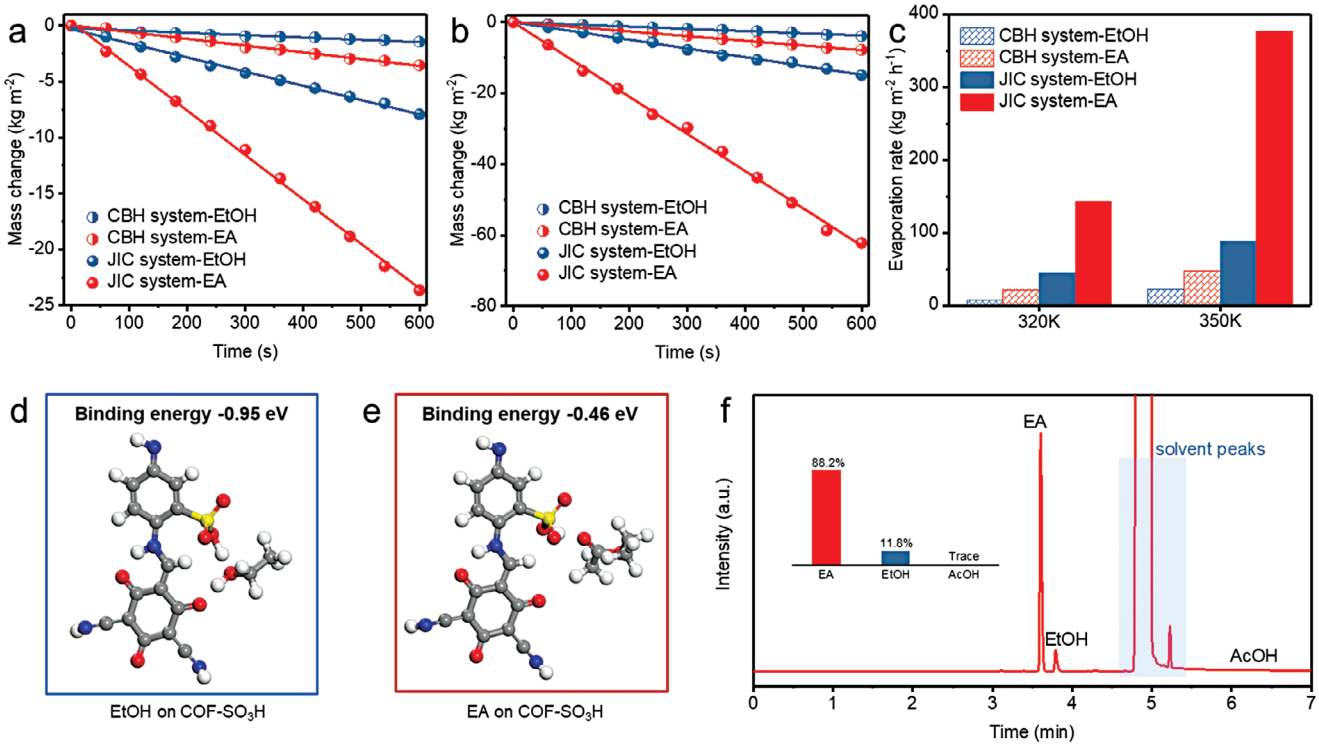

Figure 6. Mechanistic investigation of JIC system. Mass change of EtOH and EA in Different system at a) 320 K and b) 350 K (red represents EA and blue represents EtOH). c) Evaporation rates of both systems under 320 or 350 K. Optimized atomic structure of d) EtOH and e) EA on COF—SO_3H. f) GC chromatogram of the steam generated in the JIC.

recognized as a second-order reversible reaction, which is consistent with the previous report.[21] Beyond this temperature, conversion rates began to decline due to excessive heat causing rapid evaporation of reactants from the catalytic sites, thus impeding esterification performance.[22] This phenomenon indicated a specific temperature range was required in electrified esterification to optimal high conversation rate. Furthermore, the influence of varied COF—SO_3H loadings on the equilibrium conversion rate was also explored. As shown in Figure 5c, the equilibrium conversion rate of the esterification reaction continuously improved with increasing the catalyst loading. The optimal conversion rate (80.5%) was achieved at a catalyst loading of 40 mg cm^{-3}. However, excessive COF—SO_3H loading led to reduced conversion efficiency due to the aggregation of COF—SO_3H powder within the CF, resulting in decreased available acid sites.

Additionally, the influence of different reactant ratios (EtOH:AcOH) in the JIC system for electrified esterification was studied (Figure 5d). Equilibrium conversion rates can be improved by increasing reactant molar ratios, particularly exceeding 96% at a ratio surpassed 3:1 (EtOH:AcOH), which was markedly superior to the CBH system (≈42.5%). Moreover, the JIC system using COF—SO_3H@CF significantly reduced energy consumption for the esterification reaction, especially with increased reactant molar ratios (Figure 5e). Comparative analysis with literature shows that the JIC system based on the COF—SO_3H@CF catalyst, employing the Joule-heated interfacial catalysis, could achieve the excellent equilibrium conversion rates and turnover frequency (TOF) values regardless of reactant molar ratios (Figure 5f; Table S3, Supporting Information).[9]

The stability of COF—SO_3H@CF catalyst in JIC system was evaluated through five reaction cycles at 355 K and a 1:1 reactant molar ratio. Figure 5g demonstrates the minimal decrease in the equilibrium conversion rate. Besides, the morphology and structure of COF—SO_3H@CF catalyst remained intact, indicating a desirable stability (Figures S14–S16, Supporting Information). Finally, the versatility of JIC system was verified through conversion efficiency with different alcohols (methanol, isopropanol, and n-butanol) and acids (formic acid and oleic acid). The system showed satisfying conversion performances for different molar ratios (1:1 and 3:1) (Figure 5h), highlighting the broad applicability of the JIC system in diverse esterification reactions.

2.4. Mechanism Investigation

To elucidate the mechanism underlying the exceptional conversation rate of the JIC system in esterification reactions, comprehensive experiments and theoretical calculations were conducted. Frist of all, the evaporation rates of EtOH and EA were measured in both JIC and CBH systems with different temperatures (320 and 350 K), aiming to emphasize the positive contribution of JIC system on esterification reaction. It is obvious that the vapor generation rate of EtOH and EA in JIC system are much faster than those in CBH system under identical temperature (**Figures** 6a,b). Among them, the evaporation rates are calculated from the slope of mass change curve (Figures 6c). In JIC system, EA reaches an evaporation rate of 143 kg m^{-2} h^{-1} at

320 K, which is 3.1 times higher than EtOH of 45.7 kg m^{-2} h^{-1}. At 350 K, this disparity further widens, with the evaporation rate of EA (377.7 kg m^{-2} h^{-1}) being ≈4.2 times higher than EtOH (88.8 kg m^{-2} h^{-1}). While in CBH system, the evaporation rate of EA at 320 K is 21.7 kg m^{-2} h^{-1}, 2.8 times higher than EtOH (7.6 kg m^{-2} h^{-1}). When the temperature reaches 350 K, this disparity decreases, with the evaporation rate of EA (47.6 kg m^{-2} h^{-1}) being 2.1 times that of EtOH (22.6 kg m^{-2} h^{-1}). The results indicated that the JIC system is more favorable for EA evaporation with the increased temperature, compared to the CBH system. Within the JIC system, the EtOH and AcOH were transported across the CF by capillary action, subsequently catalyzed into EA. Since the enhanced evaporation rate, the product can be more efficiently evaporated away from the catalytic interface compared to the reactants. Thus, the reactants were maintained a high concentration at the catalytic interface, thereby promoting the esterification reactions forward and breaking the equilibrium limit of 62.5%. However, the evaporation rate in CBH system markedly decreased with a limited interface between the bulk solution and atmosphere. Furthermore, the resultant products tend to dissolve in reaction mixture instead of accumulating at evaporation interface, which adversely affects the efficient products separation and impedes the advanced esterification process.

We further conducted the theoretical calculation using density functional theory (DFT) to delineate differences in the evaporation rate between EA and EtOH on COF—SO_3H@CF. As illustrated in Figure 6d,e, the binding energy of EA with COF—SO_3H (−0.46 eV) was lower than that of EtOH (−0.95 eV), indicating that the EA was prone to evaporate at the catalytic interface compare to EtOH in the COF—SO_3H. Owing to the strengthened electrostatic interaction and hydrogen bonds between the —SO_3H group of COF—SO_3H and the —OH group of EtOH, the binding force between the EtOH and COF—SO_3H was stronger and made less evaporation.[17,23] Hence, at the catalytic interface, products were more prone to dissociate from the active sites, while reactants can be maintained at higher concentrations, thereby facilitating the forward progression of esterification reaction. To further confirm the content of steam during the reaction, we performed a gas chromatograph (GC) to examine the content of each substance in the steam (Figure 6f). The chromatogram revealed that the EA was the main component (88.2%), with a minor presence of EtOH (≈11.8%), and no AcOH was detected. This clearly indicates that the utilization of COF—SO_3H@CF enabled the rapid evaporation of EA from the catalytic interface, thus promoting the reaction progress. To confirm the distribution of reactants at the catalytic interface, operando attenuated total reflection surface-enhanced infrared adsorption spectroscopy (ATR-SEIRAS) was performed. As shown in Figure S17 (Supporting Information), the absorption bands of C═O (1721 cm^{-1}), O—H (1408 cm^{-1}), and C—O (1285, 1083, and 1045 cm^{-1}) in the ATR-SEIRAS spectra are correspond to the signals of AcOH and EtOH. Additionally, an EA signal (2974 cm^{-1}) was observed after the reaction commenced. With the extended reaction time, the integral area of characteristic peak for the reactant was much larger than that of the product, revealing that the reactant remained at a higher concentration at the catalytic interface during the reaction process. As a result, the JIC system can achieve in situ separation of products at the catalytic interface through the Joule heating process, which allows the reactants to maintain a relatively high concentration, thus promoting the forward progress of the esterification reaction.

3. Conclusion

In summary, we have successfully prepared a COF—SO_3H@CF catalyst with abundant acid sites by a simple hydrothermal method, and subsequently applied it to construct a JIC system for advanced electrified esterification, achieving high conversion and energy efficiency. Optimization of reaction conditions for electrified esterification enabled a conversion rate of AcOH as high as 80.5% at a heating power density of 0.49 W cm^{-3}, without additional reagents, surpassing the chemical equilibrium limitation of the esterification reaction. Comprehensive analysis involving finite element simulation, evaporation rate experiments, operando ATR-SEIRAS spectra, and DFT calculations indicated that the Joule heating effect at the catalytic interface promotes rapid evaporation of the products in JIC system. This maintains a higher concentration of reactants around the catalyst sites while keeping the product concentration lower, thereby accelerating the esterification process. This work not only significantly improves the equilibrium conversion rate of esterification but also reduces energy consumption.

Supporting Information

Supporting Information is available from the Wiley Online Library or from the author.

Acknowledgements

J.Z. and X.Z. contributed equally to this work. The authors thank the National Natural Science Foundation of China (grant no. 52102325), Collaborative Innovation Program of Hefei Science Center, CAS (grant no. 2022HSC-CIP016), and the National Natural Science Foundation of China (No. 52301271). Numerical computations were performed on Hefei Advanced Computing Center.

Conflict of Interest

The authors declare no conflict of interest.

Data Availability Statement

The data that support the findings of this study are available in the supplementary material of this article.

Keywords

covalent organic framework, electrothermal reaction, esterification reaction, interfacial catalysis, Joule heating

Received: September 16, 2024
Revised: November 2, 2024
Published online:

[1] a) S. T. Wismann, J. S. Engbæk, S. B. Vendelbo, F. B. Bendixen, W. L. Eriksen, K. Aasberg-Petersen, C. Frandsen, I. Chorkendorff, P. M. Mortensen, *Science* **2019**, *364*, 756; b) D. S. Mallapragada, Y. Dvorkin, M. A. Modestino, D. V. Esposito, W. A. Smith, B.-M. Hodge, M. P. Harold, V. M. Donnelly, A. Nuz, C. Bloomquist, K. Baker, L. C. Grabow, Y. Yan, N. N. Rajput, R. L. Hartman, E. J. Biddinger, E. S. Aydil, A. D. Taylor, *Joule* **2023**, *7*, 23; c) Q. Dong, Y. Yao, S. Cheng, K. Alexopoulos, J. Gao, S. Srinivas, Y. Wang, Y. Pei, C. Zheng, A. H. Brozena, H. Zhao, X. Wang, H. E. Toraman, B. Yang, I. G. Kevrekidis, Y. Ju, D. G. Vlachos, D. Liu, L. Hu, *Nature* **2022**, *605*, 470.

[2] a) X. Mei, X. Zhu, Y. Zhang, Z. Zhang, Z. Zhong, Y. Xin, J. Zhang, *Nat. Catal.* **2021**, *4*, 1002; b) Z. W. Seh, J. Kibsgaard, C. F. Dickens, I. Chorkendorff, J. K. Nørskov, T. F. Jaramillo, *Science* **2017**, *355*, eaad4998.

[3] a) L. Zheng, M. Ambrosetti, E. Tronconi, *ACS Eng. Au* **2023**, *4*, 4; b) W. Wang, S. Zhao, X. Tang, C. Chen, H. Yi, *Chem. Eng. J.* **2023**, *455*, 140272.

[4] L. Dou, C. Yan, L. Zhong, D. Zhang, J. Zhang, X. Li, L. Xiao, *Chem. Commun.* **2020**, *56*, 205.

[5] Q. Dong, A. D. Lele, X. Zhao, S. Li, S. Cheng, Y. Wang, M. Cui, M. Guo, A. H. Brozena, Y. Lin, T. Li, L. Xu, A. Qi, I. G. Kevrekidis, J. Mei, X. Pan, D. Liu, Y. Ju, L. Hu, *Nature* **2023**, *616*, 488.

[6] a) Z. Wang, Y. Zhang, Z. Zhang, D. Zhou, Z. Cao, Y. Sha, *Chin. J. Chem. Eng.* **2023**, *53*, 63; b) H. Huang, C. Yu, X. Han, H. Huang, Q. Wei, W. Guo, Z. Wang, J. Qiu, *Energy Environ. Sci.* **2020**, *13*, 4990.

[7] J. Han, C. A. Haines, J. J. Piane, L. L. Filien, E. D. Nacsa, *J. Am. Chem. Soc.* **2023**, *145*, 15680.

[8] a) J. Ding, S. Qu, E. Lv, J. Lu, W. Yi, *Energy Fuels* **2020**, *34*, 15614; b) B. Van Wettere, S. Aghakhani, J. Lauwaert, J. W. Thybaut, *Appl. Catal. A-Gen.* **2022**, *646*, 118849; c) M. Nielsen, H. Junge, A. Kammer, M. Beller, *Angew. Chem., Int. Ed.* **2012**, *51*, 5711.

[9] P. Yao, H. Gong, Z.-Y. Wu, H. Fu, B. Li, B. Zhu, J. Ji, X. Wang, N. Xu, C. Tang, H. Zhang, J. Zhu, *Nat. Sustain.* **2022**, *5*, 348.

[10] Y. Li, S. Han, L. Zhang, W. Li, W. Xing, *J. Membr. Sci.* **2019**, *579*, 120.

[11] a) I. Ogino, Y. Suzuki, S. R. Mukai, *ACS Catal.* **2015**, *5*, 4951; b) A. E. A. A. Said, M. N. Goda, *J. Am. Chem. Soc.* **2019**, *67*, 567; c) H. Gurav, V. V. Bokade, *J. Nat. Gas Chem.* **2010**, *19*, 161.

[12] a) L. Shi, W. Tao, N. Zheng, W. Tang, T. Zhou, Z. Sun, *Chem. Eng. J.* **2023**, *469*, 143813; b) H. Xie, N. Liu, Q. Zhang, H. Zhong, L. Guo, X. Zhao, D. Li, S. Liu, Z. Huang, A. D. Lele, A. H. Brozena, X. Wang, K. Song, S. Chen, Y. Yao, M. Chi, W. Xiong, J. Rao, M. Zhao, M. N. Shneider, J. Luo, J.-C. Zhao, Y. Ju, L. Hu, *Nature* **2023**, *623*, 964.

[13] K. Wang, Y. Zeng, W. Lin, X. Yang, Y. Cao, H. Wang, F. Peng, H. Yu, *Carbon* **2020**, *167*, 709.

[14] D. Xia, J. Mannering, P. Huang, Y. Xu, Q. Li, H. Li, Y. Qin, A. N. Kulak, R. Menzel, *J. Am. Chem. Soc.* **2023**, *146*, 159.

[15] a) Z. Xiong, B. Sun, H. Zou, R. Wang, Q. Fang, Z. Zhang, S. Qiu, *J. Am. Chem. Soc.* **2022**, *144*, 6583; b) Q. Zhang, S. Dong, P. Shao, Y. Zhu, Z. Mu, D. Sheng, T. Zhang, X. Jiang, R. Shao, Z. Ren, J. Xie, X. Feng, B. Wang, *Science* **2022**, *378*, 181; c) H. Wang, Y. Zhai, Y. Li, Y. Cao, B. Shi, R. Li, Z. Zhu, H. Jiang, Z. Guo, M. Wang, L. Chen, Y. Liu, K.-G. Zhou, F. Pan, Z. Jiang, *Nat. Commun.* **2022**, *13*, 7123.

[16] a) C. Li, J. Yang, P. Pachfule, S. Li, M.-Y. Ye, J. Schmidt, A. Thomas, *Nat. Commun.* **2020**, *11*, 4712; b) C. Jiang, Y. Zhang, M. Zhang, N.-N. Ma, G.-K. Gao, J.-H. Wang, M.-M. Zhang, Y. Chen, S.-L. Li, Y.-Q. Lan, *Cell Rep. Phys. Sci.* **2021**, *2*, 100392; c) D.-G. Wang, T. Qiu, W. Guo, Z. Liang, H. Tabassum, D. Xia, R. Zou, *Energy Environ. Sci.* **2021**, *14*, 688.

[17] C. Li, S. Cao, J. Lutzki, J. Yang, T. Konegger, F. Kleitz, A. Thomas, *J. Am. Chem. Soc.* **2022**, *144*, 3083.

[18] L. Cao, H. Wu, Y. Cao, C. Fan, R. Zhao, X. He, P. Yang, B. Shi, X. You, Z. Jiang, *Adv. Mater.* **2020**, *32*, 2005565.

[19] R. Wang, Y. Zhou, Y. Zhang, J. Xue, J. Caro, H. Wang, *Adv. Mater.* **2022**, *34*, 2204894.

[20] N. Zou, Q. Nie, X. Zhang, G. Zhang, J. Wang, P. Zhang, *Chem. Eng. J.* **2019**, *357*, 1.

[21] B. M. Antunes, S. P. Cardoso, C. M. Silva, I. Portugal, *J. Chem. Educ.* **2011**, *88*, 1178.

[22] Z. Khan, F. Javed, Z. Shamair, A. Hafeez, T. Fazal, A. Aslam, W. B. Zimmerman, F. Rehman, *J. Ind. Eng. Chem.* **2021**, *103*, 80.

[23] L. Ma, Y. Han, K. Sun, J. Lu, J. Ding, *Energy Convers. Manage.* **2015**, *98*, 46.